Earthline Journal of Mathematical Sciences
E-ISSN: 2581-8147
Volume 14, Number 2, 2024, Pages 221-242
https://doi.org/10.34198/ejms.14224.221242

Bioconvection in a Porous Medium Saturated with a Casson Nanofluid

S. O. Akhigbe* and E. O. Oghre

Department of Mathematics, University of Benin, P.M.B. 1154, Benin City, Nigeria
e-mail: stella.akhigbe@uniben.edu*

Abstract

The bio-convective heat transfer of an incompressible, viscous, electrically conducting Casson nanofluid past a wedge has been analyzed. Furthermore, using a similarity variable, the governing flow equations are transformed to non-linear coupled differential equations corresponding to a two-point boundary value problem, which is solved numerically. A comparison of the solution technique is carried out with previous work and the results are found to be in good agreement. Numerical results for the coefficient of skin friction, Nusselt number, Sherwood number, micro-organism flux as well as the velocity, temperature, nanoparticles and micro-organisms concentration profiles are presented for different physical parameters. The analysis of the obtained results shows that the field of flow is significantly influenced by these parameters.

1. Introduction

Found almost everywhere within the earth are micro-organisms. They are organisms that cannot be seen with the naked eyes except by the use of microscopes. They live in almost every habitat and are adapted to very extreme weather conditions such as extreme cold/heat. They indeed make up a vast part of life. Micro-organisms could significantly distort an ecosystem in which they are found in. The quest for a link between the microscopic world and the macroscopic world has motivated researchers, and notable discoveries have emerged. Applications exist in nanotechnology; creation of biofuels; fighting of diseases; improving of soil fertility in Agriculture amongst others. The Pioneer research work in this area can be traced in [1], who presented a theoretical result for the boundary layer flow over a flat plate in a uniform stream and on a circular

Received: October 23, 2023; Accepted: December 4, 2023; Published: January 2, 2024

2020 Mathematics Subject Classification: 76-XX.

Keywords and phrases: Sherwood number, Nusselt number, heat transfer, nanofluid, slip flow, free convection, bio-convection, similarity solution.

*Corresponding author

cylinder. The similarity solution for thermal boundary layer over a flat plate subject to convective surface boundary conditions was studied in [2]. He found out that the similarity solution for a constant convective coefficient of heat transfer does not exist. Instead, the solutions could be used as local similarity solutions. Ishak [3], further expanded [2] with no modification to the flow equations but investigated a system affected by suction and injection. He found that the surface shear stress increased due to suction, which increased the rate of heat transfer at the surface. The effects of chemical reaction on MHD flow with suction and injection was investigated in [4]. The flow equations were solved analytically using perturbation method. The team found that as the Grashof number increased so did velocity distribution. Asogwa [5] studied the numerical solution of hydromagnetic flow past an infinite vertical porous plate in presence of constant suction and heat sink. He found out that the suction parameter, heat sink parameter, Hartmann number and permeability parameter significantly affected the flow. Heat and mass transfer on a MHD flow over a semi-infinite flat plate in a porous medium was studied in [6]. The results obtained indicated that the concentration of the buoyancy effects was enhanced by the increase in Grashof number. The influence of the heat absorption on the system was that which reduced the temperature of the fluid; this resulted in decrease in the velocity of the fluid. The effects of viscosity dissipation on a viscoelastic flow over a stretching surface have been investigated in [7]. It was found that the viscosity dissipation is largely dependent on the Brinkmann's constant of the material. In [8], the influence of viscosity dependent on temperature, on a hydrodynamic flow was studied. It was studied over a surface, moving continuously. The results were obtained numerically using Runge-Kutta method to the fourth order. The results obtained revealed that as the variable viscosity parameter decreases the temperature is increased. And the velocity increases as the variable viscosity parameter decreases. In [9], the effects of injection and suction on a boundary layer were considered. The results were obtained numerically using a method similar to the method used in [10]. It was reported that, in the boundary layer the rate at which heat was transferred is greatly govern by the suction and injection parameters. Thermal radiation on a MHD flow over a flat plate of uniform heat source and sink has been investigated in [11]. It was observed that the Nusselt number increases for pertinent flow parameters. In [12], the effects of blowing and suction on a thermal boundary layer were studied. An analytical solution was obtained using perturbation method, after which, graphical representations of pertinent fluid parameters were presented. In [13], the effects of Navier slip together with Newtonian heating on a hydro magnetic flow were considered. The numerical solution of

the resulting flow equations was obtained. He found that as the flow became more unsteady and Newtonian heating increased at the boundary layer, the slip parameter significantly affected the skin friction and transfer rate of heat. A nanoparticles fluid suspension is known as nanofluid, obtained by dispersing nanometer sized particles in a conventional base fluid like water, oil, ethylene glycol etc. Nanoparticles are expected to increase the thermal conductivity and consequently the attributes of heat transfer of the base fluid [14]. An extensive analysis into convective transport in nanofluids was presented in [15]. He presented that enhancement in heat transfer was as a decrease in viscosity within the boundary layer necessitated by the introduction of nanoparticles in the fluid. In an international nanofluid property benchmark exercise (INPBE) conducted by 34 organizations participating across the world. A unanimous agreement indicating that thermal conductivity was enhanced consistently across research conducted by participants. The DuFour effects on nanofluids were discussed in [16]. They reported the influence of DuFour effects on Nusselt number for varying fluid parameters. The thermophysical properties on a MHD flow was analyzed in [17]. The study was carried out over a flat plate. The equations were solved numerically using symbolic software Mathematica 8.0. They reported that the coefficient of skin friction and local Nusselt number as well as the velocity and temperature profiles were affected by varying values of the fluid flow. The numerical solution and recommendations for the Falkner-Skan flow over a wedge was presented in [18]. MHD bioconvective nanofluid over a stretching sheet was discussed in [19]. They reported an inverse relationship between density of motile microorganisms and bioconvection Lewis number together with the stretching parameter. They reported that the mass transfer rate was higher in the porous medium and the effect of the Biot number was exactly the same for both magnetic field and porous medium. They reported that the coefficient of skin friction and local Nusselt number as well as the velocity and temperature profiles were affected by varying values of the fluid flow. The MHD flow past a permeable plate was analyzed in [20]. The chemical reaction on an unsteady MHD flow over a wedge was studied in [21]. The boundary layer flow past a wedge was investigated in [22]. They reported the effects of the flow parameters as the system was analyzed. Bioconvection in a non-Darcy porous medium was studied in [23]. The governing flow equations were solved using MATLAB ODE solver. They reported that heat, mass and motile microorganism transfer rates were greatly influenced by the bioconvection parameters. Variable surface heat flux bioconvection of a casson nanofluid was studied in [24]. They reported that the skin friction coefficient was reduced owing greatly to the inclusion of the microorganisms. The two-dimensional bio-

convective Casson nanofluid flow through a wedge is investigated. The flow equations are solved numerically, having been transformed using a suitable similarity variable. Graphical and tabular representations of important magnetohydrodynamic features of the flow are presented.

2. Formulation of the Problem

2.1. Analysis of flow

Consider the steady boundary layer MHD flow past a wedge embedded in a porous medium filled with a Casson nanofluild containing gyrotactic micro-organisms.

The nanoparticle suspension is assumed to be stable and dilute, i.e., the nanoparticle concentration is less than 1%. It is assumed that the direction of swimming and velocity of the micro-organisms is uniform and there is no production of extracellular polymers on the micro-organism surface. The base fluid is a dilute solution of nutrients in which the micro-organisms can live and flow through the porous medium. Application of the magnetic field, enhances the heat transfer due to the generated temperature gradient which can affect the solute concentration. It is assumed that the porous matrix does not absorb the micro-organisms and that the pore sizes are significantly larger than the microorganisms so that they move freely within the porous medium.

2.2. Governing equations

The coordinate system is such that x-axis is along the surface of the wedge and the y-axis is perpendicular to it. Figure 1 shows the flow configuration.

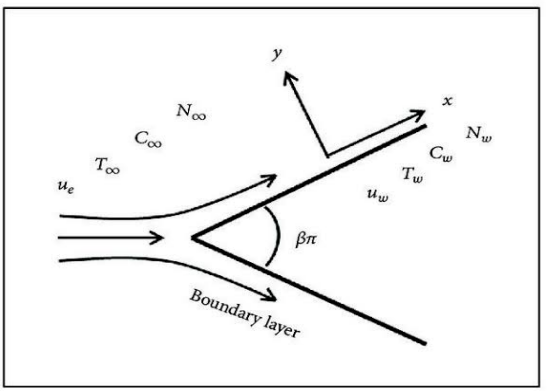

Figure 1: Sketch of flow geometry (source: [22]).

At the upper surface of the wedge, fluid flow with free stream velocity $u_e(x)$, temperature T_∞, nanoparticles concentration C_∞ and micro-organisms concentration n_∞. It is assumed that at the lower surface of wedge the temperature is T_w, nanoparticles concentration is C_w and micro-organism concentration is n_w. The fluid near the wall transfers heat, mass and micro-organisms between the wall and the fluid farther out at coefficients h_f, h_w and h_s respectively.

A uniform magnetic fluid is applied perpendicular to the flow direction and varies in strength as a function of x. Pressure gradient, viscous dissipation and thermal radiation are taken into account in the presence of heat and chemical reaction. The flow is due to buoyancy forces necessitated by the density gradients caused by temperature differences, nanoparticles distribution, and micro-organisms distribution in the medium.

As a result of the aforementioned conditions and assumptions, the governing flow equations subject to the Oberbeck-Boussinesq approximations are given by;

Continuity Equation:

$$\frac{\partial u}{\partial x}+\frac{\partial v}{\partial y}=0 \tag{1}$$

Momentum Conservation Equation:

$$u\frac{\partial u}{\partial x}+v\frac{\partial u}{\partial y}=u_e\frac{\partial u_e}{\partial x}+\nu\left(1+\frac{1}{\beta}\right)\frac{\partial^2 u}{\partial y^2}+\left[\frac{\sigma B^2(x)}{\rho}+\left(1+\frac{1}{\beta}\right)\frac{\nu\varphi}{k_1}\right](u_e-u)$$

$$+\left[(1-C_\infty)\left(\rho_{f_\infty}/\rho_f\right)\beta_T g(T-T_\infty)-\left(\frac{\rho_p-\rho_{f_\infty}}{\rho_f}\right)g(C-C_\infty)-\left(\frac{\rho_{m_\infty}-\rho_f}{\rho_f}\right)\gamma g(n-n_\infty)\right]\sin\frac{\Omega}{2} \tag{2}$$

Energy Equation:

$$u\frac{\partial T}{\partial x}+v\frac{\partial T}{\partial y}=\frac{k}{(\rho c)_p}\frac{\partial^2 T}{\partial y^2}+\tau\left[D_B\frac{\partial C}{\partial y}\frac{\partial T}{\partial y}+\frac{D_T}{T_\infty}\left(\frac{\partial T}{\partial y}\right)^2\right]+\frac{\nu}{c_p}\left(1+\frac{1}{\beta}\right)\left(\frac{\partial u}{\partial y}\right)^2-\frac{1}{(\rho c)_f}\frac{\partial q_r}{\partial y} \tag{3}$$

Nanoparticle Concentration Equation:

$$u\frac{\partial C}{\partial x}+v\frac{\partial C}{\partial y}=D_n\frac{\partial^2 C}{\partial y^2}+\frac{D_T}{T_\infty}\frac{\partial^2 T}{\partial y^2}-k_c(C-C_\infty) \tag{4}$$

Micro-organism Conservation Equation:

$$u\frac{\partial n}{\partial x}+v\frac{\partial n}{\partial y}+\frac{bW_c}{C-C_\infty}\frac{\partial}{\partial y}\left(n\frac{\partial C}{\partial y}\right)=D_n\frac{\partial^2 n}{\partial y^2} \tag{5}$$

Here, $x, y=$ Cartesian coordinates, $u, v=$ velocity components along x, y-axis respectively, $u_e=$ free stream velocity, $\nu=$ kinematic viscosity, $\beta=$ Casson parameter,

$\sigma =$ electrical conductivity, $B = B_0 x^{\frac{(m-1)}{2}}$ magnetic field strength, $B_0 =$ uniform magnetic field, $\varphi =$ porosity, $k_1 = \frac{k_0}{x^{(m-1)}}$ variable permeability of porous medium, $k_0 =$ constant permeability of porous medium, $C =$ nanoparticles concentration within the boundary, $C_\infty =$ nanoparticles concentration in the free stream, $\rho_f =$ density of the nanofluid, $\beta_T =$ volume expansion coefficient, $\rho_p =$ density of nanoparticles, $\gamma =$ average volume of micro-organisms, $T =$ fluid temperature within the boundary and in the free stream respectively, $T_\infty =$ fluid temperature in the free stream, $n =$ microorganisms concentration within the boundary and in the free stream respectively, $n_\infty =$ microorganisms concentration in the free stream, $g =$ acceleration due to gravity, $c_p =$ specific heat at constant pressure, $(\rho c)_p =$ specific heat of nanoparticle, $k =$ thermal conductivity, $\tau = (\rho c)_p/(\rho c)_f =$ ratio of heat capacities of nanoparticle and fluid, $D_B =$ Brownian diffusion coefficient, $D_T =$ thermophoretic diffusion coefficient, $(\rho c)_f =$ specific heat of fluid, $q_r =$ radiative heat flux, $D_n =$ diffusivity of micro-organisms, $T_m =$ mean fluid temperature, $k_c = ak_2 x^{m-1}$ chemical reaction parameter, $a =$ reference length along the flow, $k_2 =$ constant reaction rate, $W_c =$ maximum cell swimming speed and $b =$ chemotaxis constant.

2.3. Boundary conditions

$$u(x,y) \to u_w(x) + N_1 v\left(1+\frac{1}{\beta}\right)\frac{\partial u}{\partial y}, \quad v(x,y) = 0, \quad k\frac{\partial T}{\partial y} = -h_f(T_w - T),$$
$$D_B\frac{\partial C}{\partial y} = -h_s(c_w - C), \quad D_n\frac{\partial n}{\partial y} = -h_w(n_w - n) \qquad \text{at } y = 0 \tag{6}$$

$$u(x,y) \to u_e, \quad T(x,y) \to T_\infty, \quad C(x,y) \to C_\infty, \quad n(x,y) \to n_\infty \quad \text{as } y \to \infty \tag{7}$$

Here, $u_w(x) = U_w x^m =$ wedge velocity, $U_w =$ constant, $N_1(x) = N_0 x^{-\frac{m-1}{2}} =$ local velocity slip factor, $N_0 =$ constant velocity slip factor, $h_f(x) = h_0 x^{\frac{m-1}{2}} =$ convective heat transfer, $h_0 =$ constant convective heat transfer, $h_s(x) = h_1 x^{\frac{m-1}{2}} =$ convective mass transfer, $h_1 =$ constant convective mass transfer, $h_w(x) = h_2 x^{\frac{m-1}{2}} =$ local microorganism slip factor, $h_2 =$ constant microorganism slip factor, $T_w = T_\infty + T_0 x^{2m} =$ lower surface temperature, $T_0 =$ reference temperature, $C_w = C_\infty + C_0 x^{2m} =$ lower surface nanoparticle concentration, $C_0 =$ reference nanoparticle concentration, $n_w = n_\infty + n_0 x^{2m} =$ lower surface microorganisms concentration, $n_0 =$ reference microorganisms concentration, and $u_e(x) = U_\infty x^m =$ free stream velocity, $U_\infty =$ constant.

According to [25]

$$q_r = -\frac{4\sigma^*}{3{k_1}^*}\frac{\partial T^4}{\partial y} \tag{8}$$

is the Rosseland radiative heat flux. Here σ^* = Stefan-Boltzmann constant, ${k_1}^*$ = mean absorption coefficient. By using Taylor's series, expanding T^4 about the free stream temperature, and ignoring higher order terms, we have:

$$T^4 = {T_\infty}^4 + 4{T_\infty}^3(T - T_\infty) + 6{T_\infty}^2(T - T_\infty)^2 + \ldots$$
$$T^4 \cong 4{T_\infty}^3 T - 3{T_\infty}^4 \tag{9}$$

Substituting equations (8) and (9) in equation (3), equation (3) becomes

$$u\frac{\partial T}{\partial x} + v\frac{\partial T}{\partial y} = \left(\frac{k}{(\rho c)_p} + \frac{16\sigma^*}{3(\rho c)_f}\frac{{T_\infty}^3}{{k_1}^*}\right)\frac{\partial^2 T}{\partial y^2} + \tau\left[D_B\frac{\partial C}{\partial y}\frac{\partial T}{\partial y} + \frac{D_T}{T_\infty}\left(\frac{\partial T}{\partial y}\right)^2\right] + \frac{\nu}{c_p}\left(1 + \frac{1}{\beta}\right)\left(\frac{\partial u}{\partial y}\right)^2 \tag{10}$$

2.4. Introduction to dimensionless form

The dimensionless variables for ψ, T, C and n with respect to a similarity variable are introduced following [20] as:

$$\psi = \left(\frac{2U_e \nu x}{m+1}\right)^{\frac{1}{2}} f(\eta) \tag{11}$$

$$T = T_\infty + (T_w - T_\infty)\theta(\eta) \tag{12}$$

$$C = C_\infty + (C_w - C_\infty)\phi(\eta) \tag{13}$$

$$n = n_\infty + (n_w - n_\infty)\chi(\eta) \tag{14}$$

$$\eta = y\left(\frac{(m+1)U_e}{2x\nu}\right)^{\frac{1}{2}} \tag{15}$$

Where, ψ is the stream function, η is the similarity variable, f, θ, ϕ and χ are dimensionless stream function, temperature, nanoparticle volume fraction and density of motile microorganism respectively.

Using equations (11) to (15) as necessary, we have

$$u = \frac{\partial \psi}{\partial y} = U_\infty x^m f' \tag{16}$$

$$v = -\frac{\partial \psi}{\partial x} = -\frac{1}{2x}\sqrt{\frac{2\nu U_\infty}{(m+1)}}\, x^{\frac{m+1}{2}}[(m+1)f + \eta(m-1)f'] \tag{17}$$

Here, primes denote differentiation with respect to η. Now for equations (18) and (19), the continuity equation (1) is satisfied automatically. Using equations (11) to (17) where necessary in equations (2)-(5), we get

$$\left(1+\frac{1}{\beta}\right)f'''+f''f+\frac{2m}{(m+1)}\left(1-f'^2\right)+\frac{2}{(m+1)}(1-f')\left(M+\left(1+\frac{1}{\beta}\right)K\right)+\frac{2}{(m+1)}(\lambda_T\theta-\lambda_m\phi-\lambda_b\chi)\,sin\left(\frac{2}{m+1}\frac{\pi}{2}\right)=0 \tag{18}$$

$$\frac{1}{Pr}\left(1+\frac{4}{3}Rd\right)\theta''+\left(1+\frac{1}{\beta}\right)Ecf''^2+f\theta'-\frac{4m}{(m+1)}f'\theta+(N_b\phi'\theta'+N_t\theta'^2)=0 \tag{19}$$

$$\frac{1}{Sc}\phi''+\frac{1}{Sc}\frac{N_t}{N_b}\theta''-\left(\frac{2}{(m+1)}R+\frac{4m}{(m+1)}f'\right)\phi+f\phi'=0 \tag{20}$$

$$\chi''-Pe[\phi''(\Omega_2+\chi)+\chi'\phi']-Sb\left(\frac{4m}{(m+1)}f'\chi-f\chi'\right)=0 \tag{21}$$

$Gr=\frac{g\beta_T(1-C_\infty)\left(\rho_{f_\infty}/\rho_f\right)(T_w-T_\infty)x^3}{\upsilon^2}$ is the local Grashof number, $Gm=\frac{g^{\left(\rho_p-\rho_{f_\infty}\right)}/\rho_f(C_w-C_\infty)x^3}{\upsilon^2}$ is the modified local Grashof number 1, $Gb=\frac{g\gamma^{\left(\rho_{m_\infty}-\rho_f\right)}/\rho_f(n_w-n_\infty)x^3}{\upsilon^2}$ is the modified local Grashof number 2, $\lambda_T=\frac{Gr}{Re_x^2}$ is the thermal buoyancy parameter, $\lambda_m=\frac{Gm}{Re_x^2}$ is the nanoparticle mass buoyancy parameter, $\lambda_b=\frac{Gb}{Re_x^2}$ is the bioconvection buoyancy parameter, $Re_x=\frac{U_e x}{\upsilon}$ is the local Reynolds number, $M=\frac{\sigma {B_0}^2}{\rho U_\infty}$ is the magnetic parameter, $K=\frac{\nu\varphi}{k_0 U_\infty}$ is the porosity parameter, $Pr=\frac{\upsilon(\rho c)_p}{k_0}$ is the Prandtl number, $Rd=\frac{4\sigma*{T_\infty}^3}{kk_1{}^*}$ is the radiation number, $N_b=\frac{\tau D_B(C_w-C_\infty)}{\upsilon}$ is the Brownian motion parameter, $N_T=\frac{\tau D_T(C_w-C_\infty)}{\upsilon T_\infty}$ is the thermophoresis parameter, $Ec=\frac{{U_\infty}^2}{c_p(T_w-T_\infty)}$ is the Eckert number, $Sc=\frac{\upsilon}{D_B}$ is the Lewis number, $R=\frac{ak_2}{U_\infty}$ is the chemical reaction parameter, $Sb=\frac{\upsilon}{D_n}$ is the bioconvection Lewis number, $\Omega_2=\frac{n_\infty}{(n_w-n_\infty)}$ is the bioconvection constant.

The corresponding boundary conditions are:

$$f'(0)=\gamma_2+\delta\sqrt{\frac{(m+1)}{2}}\left(1+\frac{1}{\beta}\right)f''(0) \tag{22a}$$

$$f(0)=0 \tag{22b}$$

$$\theta'(0) = -Bi_1\sqrt{\frac{(m+1)}{2}}\big(1-\theta(0)\big) \tag{22c}$$

$$\phi'(0) = -Bi_2\sqrt{\frac{(m+1)}{2}}\big(1-\phi(0)\big) \tag{22d}$$

$$\chi'(0) = -Bi_3\sqrt{\frac{(m+1)}{2}}\big(1-\chi(0)\big) \tag{22e}$$

$$f'(\infty) = 1, \theta(\infty) = 0, \phi(\infty) = 0, \chi(\infty) = 0 \tag{23}$$

Here, $\gamma_2 = \frac{U_w}{U_\infty}$ is the wedge angle parameter, $\delta = N_0\sqrt{\nu U_\infty}$ is the slip parameter, $Bi_1 = \frac{h_0}{k}\sqrt{\frac{\nu}{U_\infty}}, Bi_2 = \frac{h_1}{k}\sqrt{\frac{\nu}{U_\infty}}, Bi_3 = \frac{h_2}{k}\sqrt{\frac{\nu}{U_\infty}}$ are Biot numbers.

2.5. Parameters of interest

The parameters of engineering interest for the present problem are the local skin friction, local Nusselt number, local Sherwood number and the micro-organism flux which indicate physically, wall shear stress, rate of heat transfer, rate of mass transfer, rate of micro-organism flux respectively. In dimensionless forms, these parameters are given by:

Skin-friction coefficient, C_f:

$$Re_x^{1/2}\, C_{f_x} = \left(1+\frac{1}{\beta}\right)\sqrt{\frac{(m+1)}{2}}f''(0) \tag{24}$$

Nusselt number, Nu:

$$Re_x^{-1/2}\, N\, u_x = -\left(1+\frac{4}{3}Rd\right)\sqrt{\frac{(m+1)}{2}}\theta'(0) \tag{25}$$

Sherwood number, Sh:

$$Re_x^{-1/2}\, S\, h_x = -\sqrt{\frac{(m+1)}{2}}\phi'(0) \tag{26}$$

Micro-organisms flux, Qn:

$$Re_x^{-1/2}\, Q\, n_x = -\sqrt{\frac{(m+1)}{2}}\chi'(0) \tag{27}$$

3. Numerical Solutions

The governing equations given in equation (18) to equation (21) subject to the boundary condition given by the equations (22) and (23) are coupled non-linear equations. The equations cannot be solved analytically thus a numerical solution is to be found. Notice that the set of equations (18)-(23) forms a two-point boundary value problem (BVP). As such, the solution is to be gotten numerically using the shooting technique.

We proceed to confirm the validity of our model. To do this, we set the fluid properties to be constants in order to make them particular forms of the equations known in literature, thereafter a comparison is made. Considering the case of no-slip at the boundary, absence of buoyancy force, magnetic field, nanoparticles and chemical reaction, i.e., this present work matches that in [2], [6] and [3]. To actually test our reduced model for accuracy, a comparison of the numerical solutions for pertinent parameters are calculated for $f''(0)$, $-\theta'(0)$ and presented on Table 1 and Table 2 respectively.

Table 1: Different values of m, when $M = K = \lambda_T = \lambda_m = \lambda_b = Pr = Rd = Ec = N_t = Sc = R = Pe = \Omega_2 = Sb = \gamma_2 = \delta = Bi_1 = Bi_2 = Bi_3 = 0, \beta \to \infty, N_b = 1$, for $f''(0)$.

m	Present results	[3]	[31]
0	0.4696	0.4696	0.4696
0.0141	0.5046	0.5046	0.5046
0.0435	0.5690	0.5690	0.5690
0.0909	0.6550	0.6550	0.6550
0.1429	0.7320	0.7320	0.7320
0.2000	0.8021	0.8021	0.8021
0.3333	0.9277	0.9277	0.9277
0.5000	1.0389	-	-
1	1.2326	1.2326	1.2326
5	1.5503	1.5504	1.5504

From Table 1 we can deduce that the numerical technique used in this work is justified. This is so because the data given in [6] and [21] and those of the present study show excellent agreement.

Table 2: Different values of Pr, when $m = M = K = \lambda_T = \lambda_m = \lambda_b = Rd = Ec = N_t = Sc = R = Pe = \Omega_2 = Sb = \gamma_2 = \delta = Bi_2 = Bi_3 = 0,\ \beta \to \infty, N_b = 1, Rd = 0.75,$ $Bi_1 = \frac{0.05}{\sqrt{2}}$ for $-\theta'(0)$.

Pr	Present results	[16]	[31]
1	0.3320	0.332173	0.3320
10	0.7281	0.72831	0.7281
100	1.5718	1.57218	1.5718
1000	3.3881	3.38809	3.3881
10000	7.3102	7.30080	7.3102

From Table 2 we can once again deduce that the numerical technique used in this work is justified. This is so because the data given in [6] and [21] and those of the present study show excellent agreement.

3.1. Results and discussion

Numerical computations have been carried out to analyze the results using the method described in the preceding section for different values of the flow parameters within the boundary layer. Only positive numbers of Grashof number are chosen, since we are considering a cooling problem. Take following [20], [21] and [23]

$\beta = 0.6, m = 0.2, M = 0.5, K = 0.4, \lambda_T = 0.5, \lambda_m = 0.4, \lambda_b = 0.5, Pr = 0.71,\ Rd = 0.8, Ec = 0.5, N_b = 0.4, N_t = 0.2, Sc = 0.2, R = 0.5, Pe = 0.2, \Omega_2 = 1, Sb = 0.5, \gamma_2 = 0.2, \delta = 0.2, Bi_1 = 0.2, Bi_2 = 0.2, Bi_3 = 0.2$

to be the default values of the parameters unless otherwise specified.

3.2. Computational results for fluid flow

The non-dimensional velocity, temperature, nanoparticles and micro-organisms concentration profiles for various parameters within the boundary layer are presented in the following figures.

3.2.1. Computational results for velocity profiles

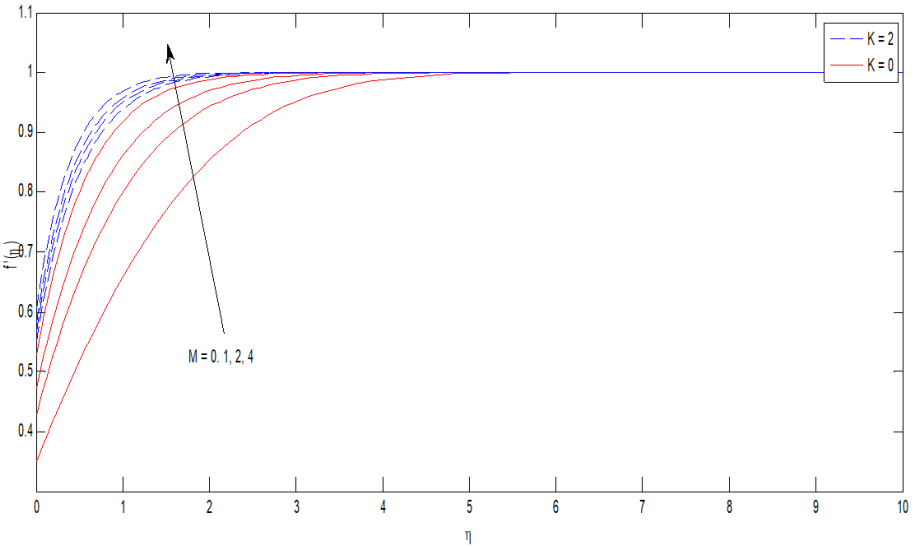

Figure 2: Effect of M on velocity profiles for different K.

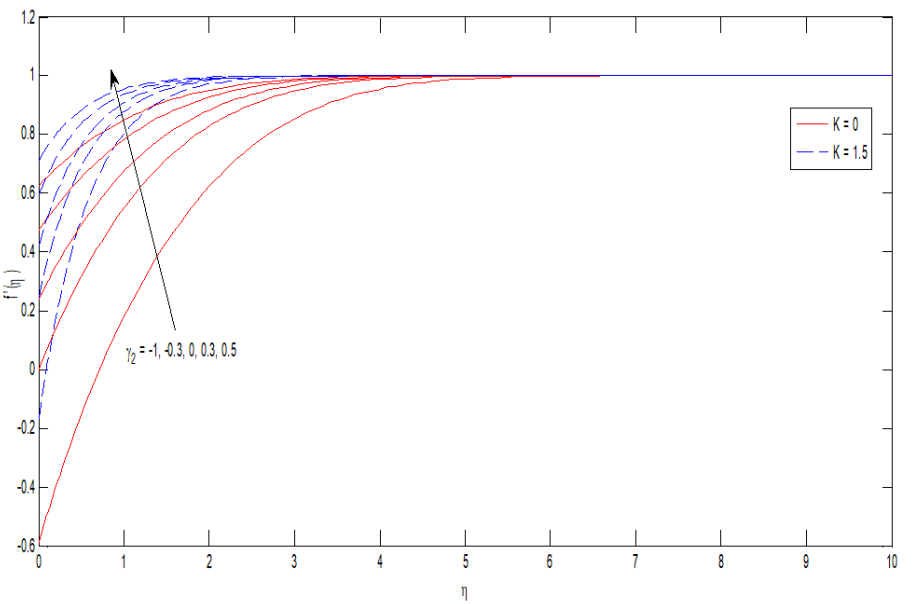

Figure 3: Effect of γ_2 on velocity profiles for different K.

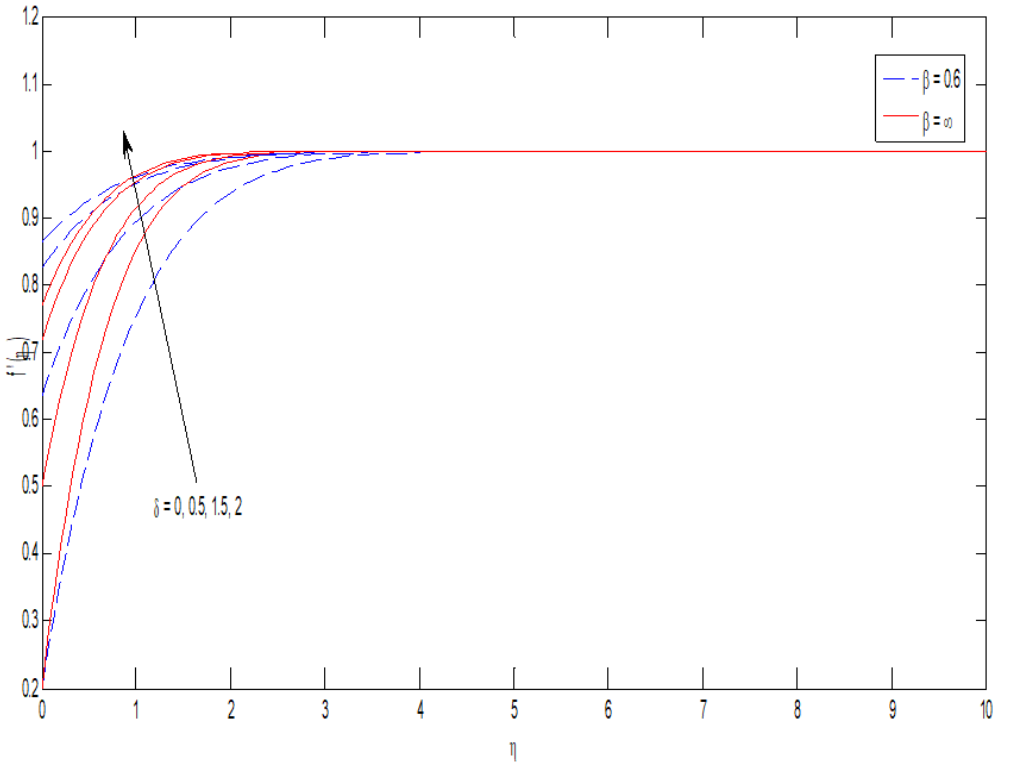

Figure 4: Effect of δ on velocity profiles for different β.

Figure 2 shows the effect of M on the velocity profile for $K = 0$, i.e., non-porous medium and $K \neq 0$ i.e., porous medium. The velocity increases as M increases. There is a strong influence of M on the velocity of fluid in the non-porous medium. An identical behavior is observed in Figure 3. The fluid velocity is much stronger in the non-porous medium as compared to the porous medium for high values of γ_2. This is as a result of the reduction in resistance by porous medium when the permeability of porous medium is increased. Figure 4 portrays the effects of δ on the velocity profile for $\beta \to \infty$ (Newtonian fluid) and $\beta = 0.6$ (Casson fluid). The velocity profiles increase as the momentum boundary layer thickness shrinks for both fluids. However, there is a sharper influence of δ on Casson fluid as compared to Newtonian fluid. Since the resistance between the wedge surface and the fluid particles rise with increase in β, the momentum boundary layer becomes thinner.

3.2.2. Computational results for temperature profiles

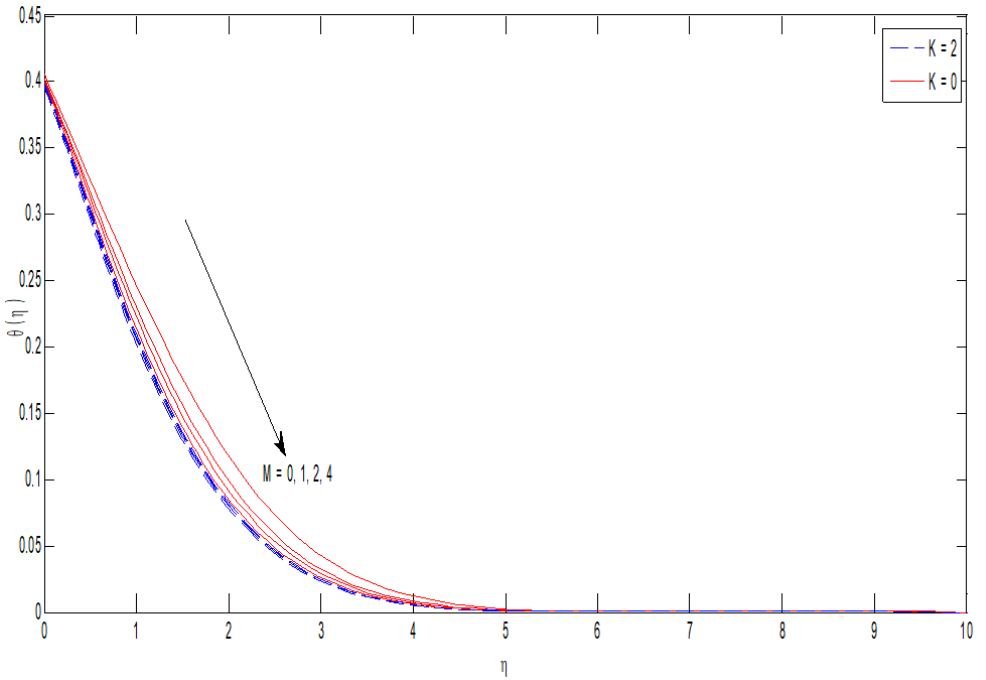

Figure 5: Effect of M on temperature profiles for different K.

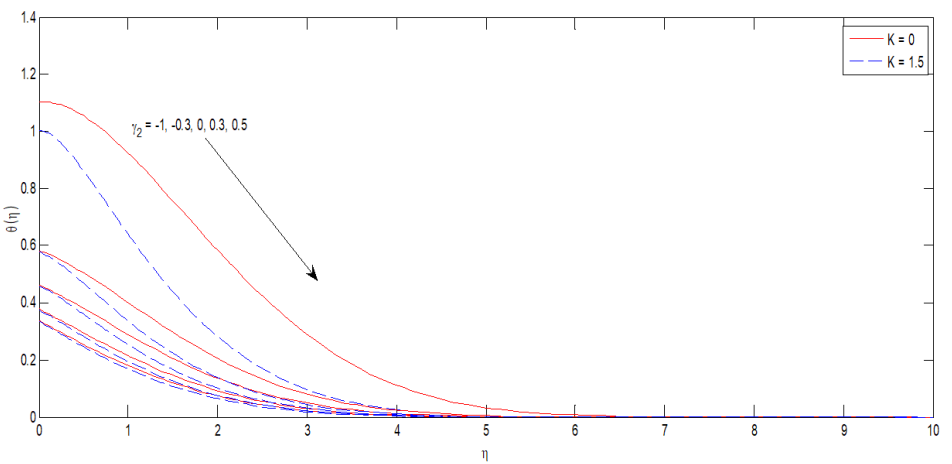

Figure 6: Effect of γ_2 on temperature profiles for different K.

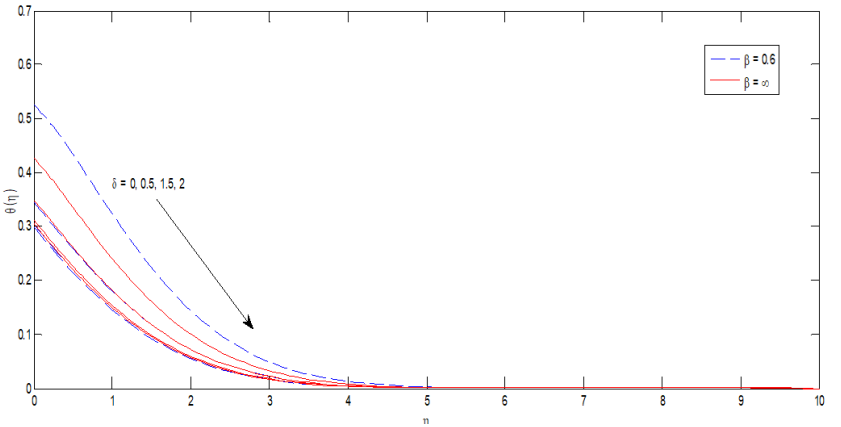

Figure 7: Effect of δ on velocity profiles for different β.

Figure 5 shows the effect of M on the temperature profile for non-porous medium and porous medium. The temperature profile reduces as M increases. Though this drop is greatly noticed in non-porous medium for large values of M. There is a higher rate of cooling in porous medium as compared to non-porous medium for high values of M. Similarly, the effect of γ_2 on the temperature profile is displayed in Figure 6. There is a reduction in the thermal boundary layer thickness for high values of γ_2 and in the porous medium as compared to non-porous medium. The effect of δ on the temperature profile for Casson fluid and Newtonian fluid is shown in Figure 7. There is a noticeable fall in temperature for increasing values of δ leading to a reduction in the thermal boundary layer thickness for both fluids.

3.2.3. Computational results for nanoparticles concentration profiles

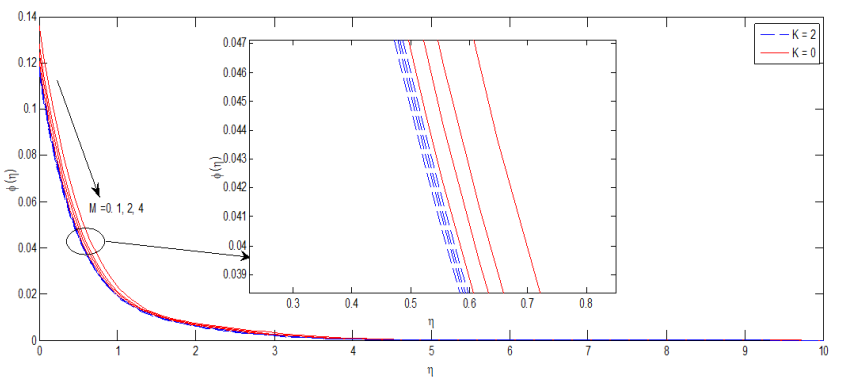

Figure 8: Effect of M on nanoparticles concentration for different K.

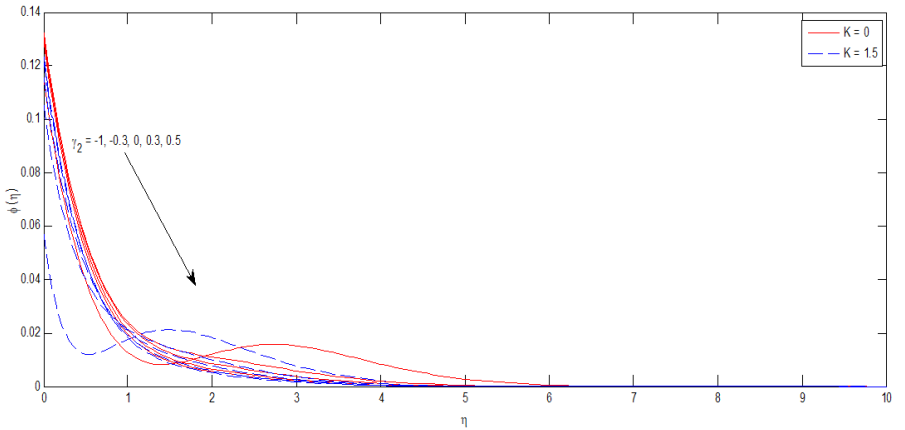

Figure 9: Effect of γ_2 on nanoparticles concentration for different K.

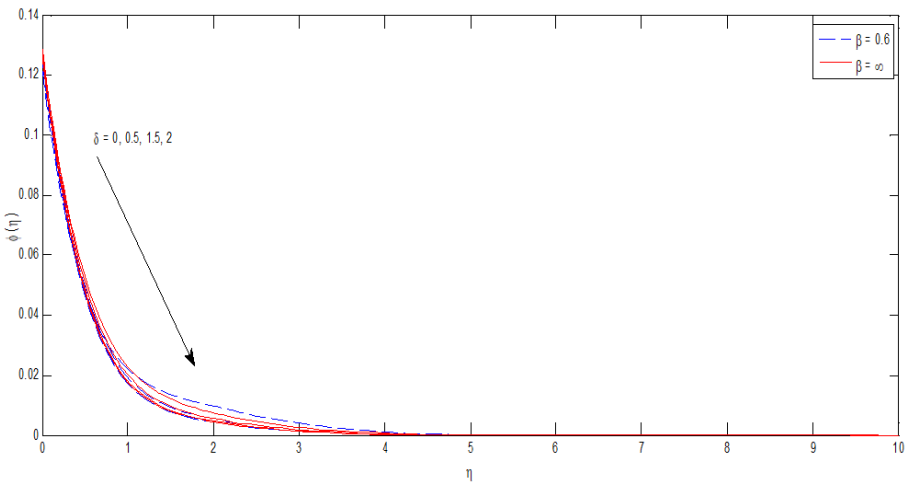

Figure 10: Effect of δ on nanoparticles concentration for different β.

Figure 8 portrays the effect of M on the nanoparticles concentration profile for non-porous medium and porous medium. The nanoparticles mass transfer rate reduces as M increases. However, the mass transfer rate is profounder in porous medium as compared to non-porous medium for high values of M. Similarly, the effect of γ_2 and δ on the nanoparticles concentration profile is displayed in Figures 9 and 10 respectively. There is a reduction in the nanoparticles concentration boundary layer thickness for the respective high values of γ_2 and δ in the porous medium and Casson as compared to non-porous medium and Newtonian fluid.

3.2.4. Computational results for micro-organisms concentration profiles

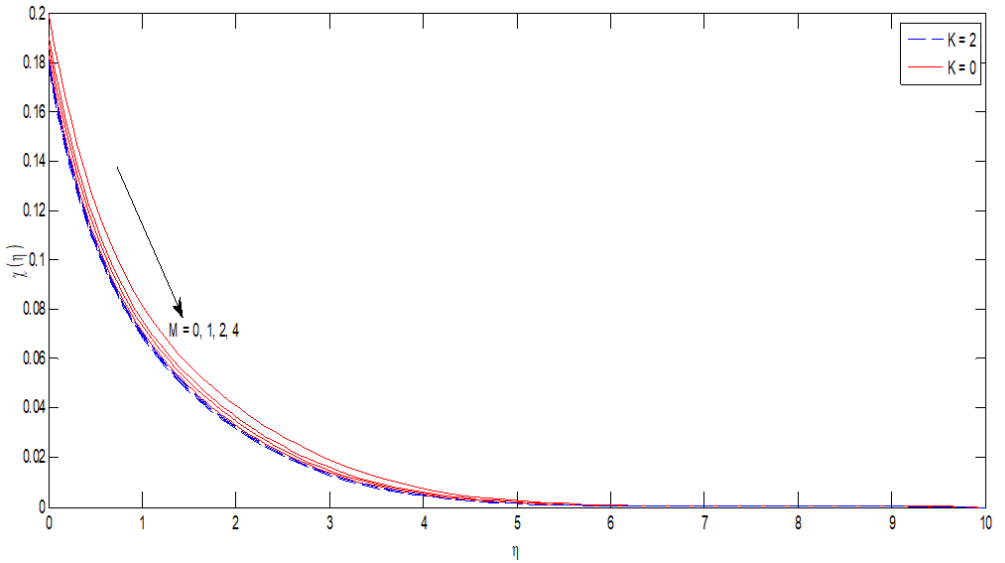

Figure 11: Effect of M on micro-organisms concentration for different K.

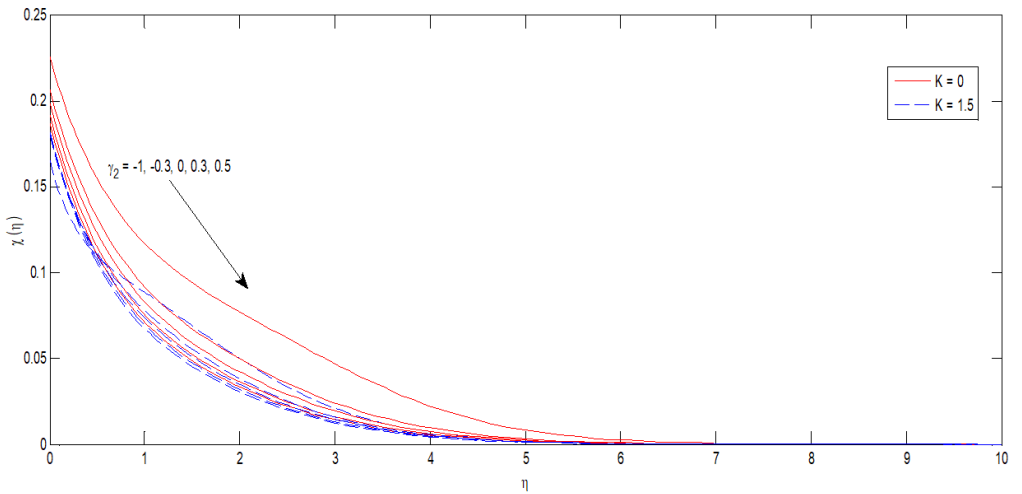

Figure 12: Effect of γ_2 on micro-organisms concentration for different K.

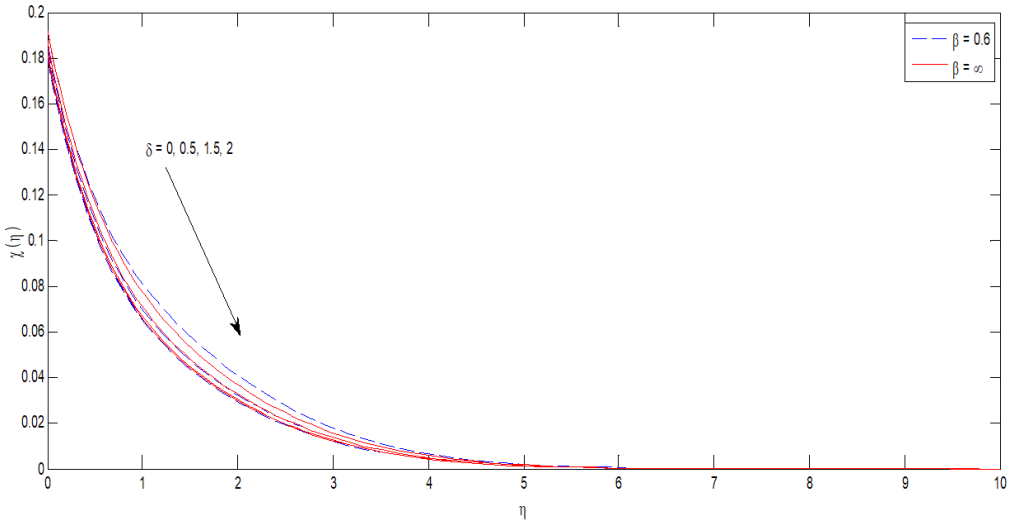

Figure 13: Effect of δ on micro-organisms concentration for different β.

Figure 11 shows the effect of M on the micro-organisms concentration profile for non-porous medium and porous medium. The micro-organisms concentration decreases as M increases. This decrease is greatly noticed in non-porous medium for large values of M. However, the micro-organisms transfer rate is stronger in porous medium as compared to non-porous medium for high values of M. Similarly, the effect of γ_2 on the micro-organisms concentration profile is displayed in Figure 12. There is a reduction in the micro-organisms boundary layer thickness for high values of γ_2 and in the porous medium as compared to non-porous medium. The effect of δ on the micro-organisms concentration profile for Casson fluid and Newtonian fluid is shown in Figure 13. The micro-organisms transfer rate decreases for increasing values of δ leading to a reduction in the micro-organisms boundary layer thickness for both fluids.

The parameters of engineering interest are calculated and presented in Table 3.

Table 3: Values of $f''(0)$, $\theta(0)$, $-\theta'(0)$, $-\phi'(0)$ and $-\chi'(0)$ for different values of β, Pr, Sc, Pe and Sb

Parameters					$\gamma_2 = 0$				$\gamma_2 = 0.5$			
β	Pr	Sc	Pe	Sb	$f''(0)$	- θ (0)	- ϕ (0)	- χ (0)	$f''(0)$	- θ (0)	- ϕ (0)	- χ (0)
0.6	0.71	0	0	0.01	0.7908	0.1386	0.0388	0.0874	0.4149	0.1714	0.0224	0.0886
0.6	1	0	0	0.5	0.7825	0.1391	0.0386	0.1834	0.4069	0.1781	0.0191	0.1899
0.6	7	0	0	1.0	0.7811	0.0959	0.0602	0.1984	0.4082	0.1982	0.0090	0.2051
0.6	11.4	0	0	10.0	0.7787	0.0716	0.0723	0.2327	0.4069	0.1987	0.0088	0.2378
0.6	0.71	0	0.2	0.01	0.7911	0.1386	0.0388	0.0854	0.4153	0.1714	0.0224	0.0833
0.6	1	0	0.2	0.5	0.7825	0.1390	0.0386	0.1841	0.4069	0.1781	0.0191	0.1891
0.6	7	0	0.2	1.0	0.7810	0.0959	0.0602	0.2020	0.4083	0.1982	0.0090	0.2045
0.6	11.4	0	0.2	10.0	0.7787	0.0716	0.0723	0.2351	0.4069	0.1987	0.0088	0.2379
0.6	0.71	3	0.2	0.01	0.7752	0.1388	0.2313	0.1174	0.3989	0.1712	0.2312	0.1183
0.6	1	3	0.2	0.5	0.7687	0.1391	0.2321	0.1912	0.3926	0.1779	0.2311	0.1966
0.6	7	3	0.2	1.0	0.7671	0.0908	0.2464	0.2055	0.3934	0.1974	0.2318	0.2097
0.6	11.4	3	0.2	10.0	0.7647	0.0607	0.2545	0.2354	0.3922	0.1974	0.2326	0.2388
1	0.71	3	0.2	0.01	0.8877	0.1406	0.2310	0.1174	0.4601	0.1716	0.2311	0.1183
1	1	3	0.2	0.5	0.8790	0.1412	0.2317	0.1908	0.4517	0.1783	0.2310	0.1965
1	7	3	0.2	1.0	0.8767	0.0941	0.2461	0.2050	0.4529	0.1980	0.2317	0.2096
1	11.4	3	0.2	10.0	0.8734	0.0636	0.2544	0.2347	0.4512	0.1981	0.2325	0.2387
∞	0.71	3	0.2	0.01	1.2251	0.1470	0.2303	0.1174	0.6471	0.1731	0.2309	0.1183
∞	1	3	0.2	0.5	1.2091	0.1487	0.2309	0.1908	0.6316	0.1800	0.2308	0.1965
∞	7	3	0.2	1.0	1.2051	0.1104	0.2443	0.2046	0.6340	0.2008	0.2313	0.2095
∞	11.4	3	0.2	10.0	1.1985	0.0820	0.2523	0.2337	0.6306	0.2012	0.2321	0.2384

From Table 3, observe that the skin friction of a Casson fluid is lower than that of a Newtonian fluid. The skin friction increases as Pe increases and reduces for high γ_2 and Sc. It is also noticed that the Nusselt number is higher for a Newtonian fluid than Casson fluid. The Nusselt number increases for high γ_2. The Sherwood number as well as the micro-organisms swimming rate are increased for high γ_2 and for Casson fluid.

4. Conclusion

The magnetohydrodynamic flow of a viscous incompressible electrically conducting Casson nanofluid over a wedge embedded in a porous medium having convective boundary condition is studied. Non-dimensional velocity, temperature, nanoparticles concentration and micro-organisms concentration profiles within the boundary layer are displayed. Presented in tabular form are the skin friction, rate of heat, mass and micro-organisms transfer from the plate to the fluid for different values of the pertinent parameters governing the flow. The following conclusions can be made from the present study:

1. The fluid velocity is much stronger in the non-porous medium.

2. There is a higher rate of cooling in porous medium compared to non-porous medium for high values of M.

3. The nanoparticles and micro-organisms concentration profiles reduce as M increases.

4. The coefficient of skin friction increases as Pe increases and reduces for high γ_2 as well as for high Sc.

5. Nusselt number and Sherwood number both increase as γ_2 is increased. Casson fluid has a high Sherwood number in comparison to Newtonian fluid.

The micro-organisms swimming rate is higher for Casson fluids in comparison to Newtonian fluids. The micro-organisms swimming rate is also significantly high for increasing γ_2.

References

[1] Blasius, H. (1908). Grenzschichten in Flüssigkeiten mit kleiner Reibung (translated version). *Z. Math-phys*, 56, 1-37.

[2] Aziz, A. (2009). A similarity solution for laminar thermal boundary layer over a flat plate with a convective surface boundary condition. *Commun. Nonlinear Sci. Numer. Simulat.*, 14, 1064-1068. https://doi.org/10.1016/j.cnsns.2008.05.003

[3] Ishak, A. (2010). Similarity Solutions for flow and heat transfer over a permeable surface with convective boundary condition. *Applied Mathematics and Computation*, 217, 837-842. https://doi.org/10.1016/j.amc.2010.06.026

[4] Ahmad, S. K., Isah, B. Y., & Altine, M. M. (2008). Chemical reaction effect on natural convective flow between fixed vertical plates with suction and injection. *Nigerian Association of Mathematical Physics*, 36, 131-140.

[5] Asogwa. (2017). Numerical solution of hydromagnetic flow past an infinite vertical porous plate. *Transactions of the Nigerian Association of Mathematical Physics*, 4, 143-150.

[6] Chamkha, A. J. (2004). Unsteady MHD convective heat and mass transfer past a semi-infinite vertical permeable moving plate with heat absorption. *International Journal of Engineering Science*, 42, 217-230. https://doi.org/10.1016/S0020-7225(03)00285-4

[7] Oghre, E. O., & Ayeni, R. O. (2002). Viscous dissipation effect in a viscoelastic flow over a stretching surface. *Nigerian Journal of Engineering Research and Development*, 1, 28-36.

[8] Elbashbeshy, E. M. A., & Bazid, M. A. A. (2000). The effect of temperature-dependent viscosity on the heat transfer over a continuous moving surface. *J. Phys. D: Appl. Phys.*, 33, 2716–2721. https://doi.org/10.1088/0022-3727/33/21/309

[9] Olanrewaju, P. O., & Makinde, O. D. (2012). Effects of thermal diffusion and diffusion thermo on chemically reacting MHD boundary layer flow of heat and mass transfer past a moving vertical plate with suction/injection. *Arabian Journal for Science and Engineering*, 36, 1607-1619. https://doi.org/10.1007/s13369-011-0143-8

[10] Karim, M. E., & Uddin, M. J. (2011). Steady radiative free convection flow along a vertical flat plate in the presence of magnetic field. *Daffodil International University Journal of Science and Technology*, 6, 55-62. https://doi.org/10.3329/diujst.v6i2.9346

[11] Das, K. (2012). Impact of thermal radiation on MHD slip flow over a flat plate with variable fluid properties. *Heat Mass Transfer*, 48, 767-778. https://doi.org/10.1007/s00231-011-0924-3

[12] Chaim, T. C. (1998). Heat transfer in a fluid with variable thermal conductivity over a linearly stretching sheet. *Acta Mechanica*, 19, 63-72. https://doi.org/10.1007/BF01379650

[13] Makinde, O. D. (2012). Computational modelling of MHD unsteady flow and heat transfer toward a flat plate with Navier slip and newtonian heating. *Brazilian Journal of Chemical Engineering*, 29, 159-166. https://doi.org/10.1590/S0104-66322012000100017

[14] Helmy, K. A. (1995). MHD boundary layer equations for power-law fluids with variable electric conductivity. *Meccanica*, 30, 187-200. https://doi.org/10.1007/BF00990456

[15] Das, K., Jana, S., & Kundu, P. K. (2015). Thermophoretic MHD slip flow over a permeable surface with variable fluid properties. *Alexandria Engineering Journal*, 54, 35-44. https://doi.org/10.1016/j.aej.2014.11.005

[16] Pakravan, H. A., & Yaghoubi, M. (2011). Combined thermophoresis, Brownian motion and Dufour effects on natural convection of nanofluids. *Int. J. of Thermal Sciences*, 50, 394-402. https://doi.org/10.1016/j.ijthermalsci.2010.03.007

[17] Akhigbe, S., & Oghre, E. O. (2017). Effects of thermophysical properties on a magnetohydrodynamic flow over a flat plate. *Transactions of Nigerian Association of Mathematical Physics*, 4, 234-241.

[18] Mohammad, M. K., & Mohammad, E. (2013). Numerical Solution for the Falkner-Skan Boundary Layer Viscous Flow over a Wedge. *Int. J. Eng. Sci*, 10, 18-36.

[19] Khan, W. A., & Makinde, O. D. (2014). MHD nanofluid bioconvection due to gyrotactic microorganisms over a convectively stretching sheet. *Int. J. of Thermal Sciences*, 81, 118-124. https://doi.org/10.1016/j.ijthermalsci.2014.03.009

[20] Jana, S., & Das, K. (2015). Influence of variable fluid properties, thermal radiation and chemical reaction on MHD slip flow over a flat plate. *Italian Journal of Pure and Applied Mathematics*, 34, 29-44.

[21] Ullah, I., Shafie, S., Makinde, O. D., & Khan, I. (2017). Unsteady MHD Falkner-Skan flow of Casson nanofluid with generative/destructive chemical reaction. *Chemical Engineering Science*, 172, 694-706. https://doi.org/10.1016/j.ces.2017.07.011

[22] Khan, W. A., & Pop, I. (2013). Boundary layer flow past a wedge moving in a nanofluid. *Mathematical Problems in Engineering*, 2013, Art. ID 637285, 7 pp. https://doi.org/10.1155/2013/637285

[23] Shaw, S., Kameswaran, P. K., Narayana, M., & Sibanda, P. (2014). Bioconvection in a non-Darcy porous medium saturated with a nanofluid and oxytactic microorganisms. *Int. J. Biomathematics*, 7, 1450005. https://doi.org/10.1142/S1793524514500053

[24] Oyelakin, I. S., Mondal, S., Sibanda, P., & Sibanda, D. (2019). Bioconvection in Casson nanofluid flow with gyrotactic microorganisms and variable surface heat flux. *Int. J. Biomathematics* 12, 1950041. https://doi.org/10.1142/S1793524519500414

[25] Atif, S. M., Hussain, S., & Sagheer, M. (2019). Magentohydrodynamic stratified bioconvective flow of micropolar nanofluid due to gyrotactic microorganisms. *AIP Advances*, 9, 025208. https://doi.org/10.1063/1.5085742